Atomic oxygen reactions with semifluorinated and *n*-alkanethiolate self-assembled monolayers

Cite as: J. Chem. Phys. **120**, 3799 (2004); https://doi.org/10.1063/1.1640336
Submitted: 01 July 2003 . Accepted: 17 November 2003 . Published Online: 20 February 2004

A. J. Wagner, G. M. Wolfe, and D. H. Fairbrother

Atomic oxygen reactions with semifluorinated and *n*-alkanethiolate self-assembled monolayers

A. J. Wagner, G. M. Wolfe, and D. H. Fairbrother[a)]
Department of Chemistry and the Department of Materials Science and Engineering, Johns Hopkins University, Baltimore, Maryland 21218

(Received 1 July 2003; accepted 17 November 2003)

The interaction of atomic oxygen ($O(^3P)$) with semifluorinated self-assembled monolayers (CF-SAMs), two different *n*-alkanethiolate self-assembled monolayers, and a carbonaceous overlayer derived from an x-ray modified *n*-alkanethiolate SAM have been studied using *in situ* x-ray photoelectron spectroscopy. For short atomic oxygen exposures, CF-SAMs remain intact, an effect ascribed to the inertness of C–F and C–C bonds toward atomic oxygen and the well-ordered structure of the CF-SAMs. Following this initial induction period, atomic oxygen permeates through the $CF_3(CF_2)_7$ overlayer and initiates reactions at the film/substrate interface, evidenced by the formation of sulfonate (RSO_3) species and Au_2O_3. These reactions lead to the desorption of intact adsorbate chains, evidenced by the loss of carbon and fluorine from the film while the C(1*s*) spectral envelope and the C(1*s*)/F(1*s*) ratio remain virtually constant. In contrast, the reactivity of atomic oxygen with alkanethiolate SAMs is initiated at the vacuum/film interface, producing oxygen-containing carbon functional groups. Subsequent reactions of these new species with atomic oxygen lead to erosion of the hydrocarbon film. Experiments on the different hydrocarbon-based films reveal that the atomic oxygen-induced kinetics are influenced by the thickness as well as the structural and chemical characteristics of the hydrocarbon overlayer. Results from this investigation are also discussed in the context of material erosion by AO in low Earth orbit. [DOI: 10.1063/1.1640336]

I. INTRODUCTION

The reactions of radical and atomic species with surfaces are important in situations including plasma etching,[1] plasma-enhanced chemical vapor deposition,[2] and thin film deposition.[3,4] Despite the importance of radicals in these technologically significant processes, the underlying molecular level events associated with radical–surface interactions are poorly understood.[5] As a result, plasma processes, including semiconductor etching and polymer modification strategies, have been developed from empirical observations. Atomic oxygen (AO) interactions with organic films represent a particularly important class of radical–surface reactions. For example, oxygen radical–surface collisions are a component of oxygen plasma treatments that are used to enhance adhesion[6] and biocompatibility.[7] Similarly, as a result of the importance of silicon oxidation and the use of oxygen plasmas in semiconductor processing, studies of AO reactions with clean silicon,[8] fused silica,[9] and hydrocarbon terminated Si(100) surfaces[10] have also been reported.

AO [predominantly ground state, $O(^3P)$] produced from the UV dissociation of molecular oxygen is also the most abundant species (10^8–10^9 cm^{-3}) encountered by spacecraft, including the space shuttle and the International Space Station, in low Earth orbit (LEO) at altitudes between 150 and 1000 km above the Earth.[11,12] It is now well established that polymers used as spacecraft coatings are degraded after exposure to LEO.[13–16] In response to this phenomena, a large number of ground-based laboratory studies have been carried out on various polymers [e.g., Kapton, FEP Teflon, Polyethylene, Polyethersulfone (PES) and Polyvinylidene fluoride (PVDF)][13–15,17–23] to determine the effects of AO exposure on organic polymers used on spacecraft as thermal control blankets, solar arrays, and second surface mirrors.[24] Despite these efforts, no clear understanding of the elementary reaction steps has emerged[12] due to the complexity of the LEO environment (containing VUV and UV radiation, AO, as well as lower concentrations of species that include O^+, NO^+, N_2, H, and O_2)[25,26] and the often complex and heterogeneous nature of the polymeric substrates employed on spacecraft in LEO. A further complication arises from the need to generate hyperthermal AO, since gas phase species in LEO strikes a spacecraft's surface with mean impact energies of approximately 4.5 eV due to the impressed velocity of the orbiting vehicle.[25] In LEO the synergistic interaction of VUV/UV irradiation and oxygen (either molecular or atomic) can also produce volatile species, whose production would contribute to the observed mass loss of fluoropolymers.[18]

As a result of these complications, recent investigations have been directed toward understanding the molecular events responsible for mass loss and film erosion of polymers exposed to various reactive components of the LEO environment using model systems.[27–30] For example, recent theoretical studies have focused on the potential for hyperthermal $O(^3P)$ atoms to initiate direct carbon–carbon chain

a)Author to whom correspondence should be addressed. Electronic mail: howardf@jhu.edu

bond breaking in hydrocarbons and fluorocarbons using ethane and hexafluoroethane as model compounds for polyethylene and fluoropolymers (e.g., Teflon), respectively.[31,32] Results from this study suggest that the $O(^3P)$ species in LEO are capable of initiating chain breaking in both hydrocarbon and fluorocarbon materials.

In experimental studies of polymer surface processes, one recent development has been the application of self-assembled monolayers (SAMs) as models for polymeric interfaces.[33–39] SAMs are well-defined organic interfaces that exhibit a number of desirable characteristics for surface studies. For example, in electron-based surface spectroscopic analysis (e.g., XPS) of SAMs, changes in the interfacial region can be accurately quantified in the absence of an often overwhelming background signal associated with the bulk.[33] Similarly, the ultrathin nature of these monolayers (typically <50 Å) eliminates the unwanted effects of charging during interactions of charged particles (ions or electrons) with the film and also enables changes in the substrate signal to be employed to quantify changes in film thickness during reactions.[37] The validity of employing SAMs as models for polymeric interfaces is also highlighted by the fact that for a common reactive species (e.g., AO) the measured recession rates of alkanethiolate SAMs and PE have been shown to be comparable (within an order of magnitude).[17,36,40] Despite these advantages SAMs do possess some experimental limitations, most notably their instability toward x-ray or electron beam exposure.[41–44]

A number of studies have explored the reactions of oxygen plasmas and reactive oxygen species $[O(^3P), O^+]$ with self-assembled monolayers (SAMs).[35–37,45] For example, George *et al.* have studied the effect of O_2 plasmas on octadecanethiolate SAMs adsorbed on gold.[35,36] Using mesh and glass baffles to remove selected reactive species within the plasma, they observed a much slower oxidation and etching rate when ions and UV/VUV radiation were removed from the plasma discharge. Results from these studies led the authors to conclude that a balance exists between substrate etching and oxidation. Etching of the film was attributed to the ions present in the plasma, while oxidation was a result of reactions involving $O(^3P)$ and O_2. More recently, Jacobs and co-workers have studied the reactions of hyperthermal ($E=5$ eV) O^+ ions with a decanethiolate SAM adsorbed on Au(111).[37] XPS analysis revealed that the incorporation of oxygen into the film competes with erosion. For hyperthermal O^+ ions, the rate of carbon removal was found to be ≈ 3 times greater than for the hyperthermal $O(^3P)$ species but 100–1000 times greater compared to recession rates measured for the thermal $O(^3P)$ species. The enhanced reactivity of the hyperthermal O^+ species is believed to result from a combination of the enhanced chemical reactivity inherent in charged particles and the increased impact energy of hyperthermal species.

In a previous study we have carried out a detailed mechanistic study of the interaction of AO generated by thermal dissociation of molecular O_2 with an x-ray modified hydrocarbon film using *in situ* XPS.[40] The film was stabilized toward further degradation and chemical modification during XPS analysis by the initial period of x-ray exposure, enabling the evolution of a single film under the influence of AO to be followed. During the earliest stages of the reaction, the dynamics of AO interactions with the film are dominated by the incorporation of new oxygen-containing functionality at the vacuum/film interface. Once a steady-state concentration of C–O, C═O, and O–C═O groups has been established, the production of volatile carbon containing species, including CO_2, is responsible for etching the hydrocarbon film. Under these conditions, the rate of carbon desorption is constant due to the fact that the effective diffusion length of oxygen radicals in the film is less than the thickness of the hydrocarbon film. Upon prolonged exposures, AO penetrates the film/substrate interface, producing Au_2O_3 and sulfonate (RSO_3) species, whereupon the loss of carbon from the film exhibits pseudo-first-order kinetics due to the limited thickness of the remaining overlayer.

In the present study, we report on the reaction of AO with a semifluorinated self-assembled monolayer (CF-SAM), dodecanethiolate and hexadecanethiolate *n*-alkanethiolate SAMs, and an x-ray modified hydrocarbon film derived from hexadecanethiolate, using *in situ* XPS. AO reactions with the CF-SAM are characterized by an induction period due to the ordered nature of the film and the chemical inertness of the C–C and C–F bonds toward direct reactions with AO. Once AO permeates through the overlayer, reactivity within the CF-SAM is initiated by O atom reactions at the film/substrate interface, leading to the production of Au_2O_3 and RSO_3 species and desorption of intact adsorbate chains. In contrast, reactions with the *n*-alkanethiolate films are initiated at the vacuum/film interface and lead to the desorption of volatile carbon-containing species and the formation of an etch front. The carbon desorption kinetics are found to be sensitive to the thickness, structural, and chemical characteristics of the hydrocarbon films.

II. EXPERIMENT

A. Sample preparation

SAMs were prepared by immersing Ar^+ sputter-cleaned polycrystalline gold substrates in a 5 mM ethanol solution of (i) 1H, 1H, 2H, 2H-perfluorodecanethiol ($CF_3(CF_2)_7(CH_2)_2SH$) for CF-SAMs,[42] (ii) dodecanethiol ($CH_3(CH_2)_{11}SH$) for C_{12}-SAMs, or (iii) hexadecanethiol ($CH_3(CH_2)_{15}SH$) for C_{16}-SAMs,[41] each for a period of 12–24 h. Gold substrates were then removed from the thiol solution and rinsed with ethanol, hexanes, and water prior to insertion into an ultrahigh vacuum (UHV) chamber. X-ray modified SAMs that comprise a cross-linked carbonaceous structure were formed by exposing pristine C_{16}-SAMs to x rays for an extended period of time (16 h) and then stored under UHV conditions for at least 20 h before exposure to AO.[40]

X-ray irradiation is known to initiate electron-stimulated C–F, C–H, C–C and S–Au bond breaking within SAMs.[41–44] These bond breaking processes compromise the structural integrity of the SAM.[41] Therefore, to minimize the effects of x-ray irradiation in the present investigation, XPS analysis was carried out on SAMs only after exposure to AO. Furthermore, each SAM was only used for a single AO ex-

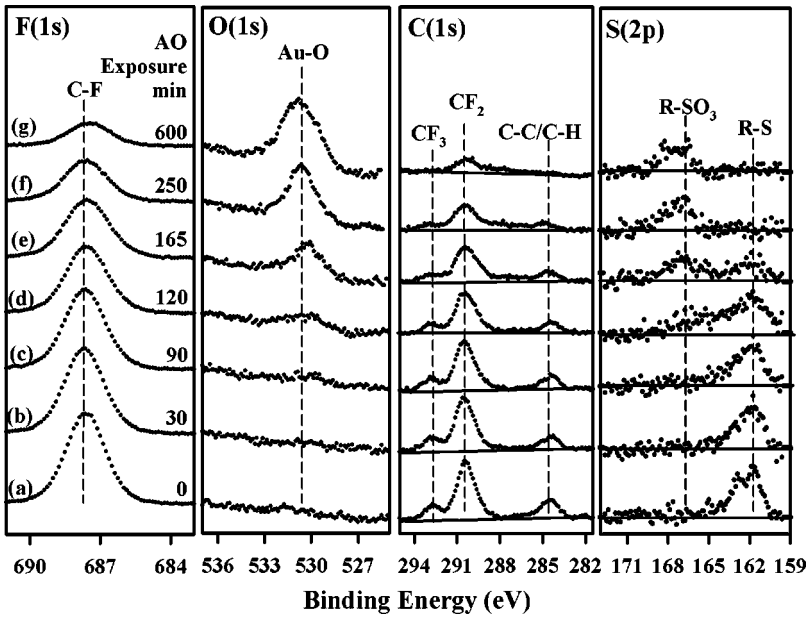

FIG. 1. Variation in the F(1*s*), O(1*s*), C(1*s*), and S(2*p*) XPS regions of a CF-SAM $[CF_3(CF_2)_7(CH_2)_2S–Au]$ as a function of AO exposure; (a) 0 min, (b) 30 min, (c) 90 min, (d) 120 min, (e) 165 min, (f) 250 min, and (g) 600 min. XPS peaks in the native CF-SAM are (i) C–F species at ≈688 eV in the F(1*s*) region; (ii) CF_3 (292.8 eV), CF_2 (290.2 eV), and C–C/C–H (284.5 eV) groups in the C(1*s*) region; and (iii) native thiolate R–S species ($2p_{3/2}$ peak at 161.8 eV). Products of the interaction of AO with the CF-SAM correspond to the Au_2O_3 peak at 530.2 eV in the O(1*s*) region and sulphonate ($R–SO_3$) species [($2p_{3/2}$) peak at 166.9 eV]. The backgrounds in the C(1*s*) and S(2*p*) regions are shown as solid lines. Each XP spectra shown in Fig. 1 corresponds to results obtained on a separately prepared CF-SAM that was analyzed by XPS only after AO exposure.

posure and then discarded; therefore, the results shown in this investigation correspond to single exposures of AO to numerous SAMs. In this context the systematic variations in the chemical composition of the CF-SAMs, the C_{12}-SAMs and the C_{16}-SAMs observed as a function of increasing exposure to AO (Figs. 1–5) are a reflection of the reproducibility of the chemical and physical properties of the native SAMs. Experiments carried out on x-ray modified C_{16}-SAMs were the only exception, owing to their stability toward additional x-ray exposure.[40] Thus, measurements reported on the x-ray modified C_{16}-SAMs were carried out on a single sample.

B. Sample analysis

In situ x-ray photoelectron spectroscopy (XPS) measurements were carried out in an UHV chamber ($P_{base} \approx 5 \times 10^{-8}$ Torr) containing the AO source.[40,46] XP spectra were acquired using a Mg K_α (1253.6 eV) x-ray source operating at 15 kV and 300 W with a take-off angle of 45° from the sample normal. XP spectra were acquired using a pass energy of 44.75 eV and a step size of 0.125 eV/step. For experiments involving the CF-SAM binding energy scales were referenced to the CF_2 peak at 290.2 eV, while for the various hydrocarbon films the C–C/C–H peak position at 284.5 eV was used. XPS data analysis was performed using commercially available software employing 100% Gaussian peaks and linear baseline subtraction.

C. Oxygen radical/atom source

AO was generated using a Thermal Gas Cracker TC-50 (Oxford Applied Research) positioned in a line of sight to the sample (target-to-sample distance of ~5 cm), as described previously.[46] The gas cracker works by passing molecular oxygen through a metallic capillary, which is heated to ≈1000 °C by electron beam irradiation. The heated capillary causes molecular oxygen to dissociate into a stream of atomic, low-energy reactive species, notably $O(^3P)$.[47] Under these conditions the AO species are assumed to have thermalized with the heated capillary, and thus possess an average kinetic energy of $kT_{capillary}$ (≈0.11 eV) during subsequent surface reactions. All of the experiments carried out as part of this investigation were carried out with the AO source operating at 45 W and a chamber pressure of $\approx 6 \times 10^{-7}$ Torr. The source was calibrated and the flux of AO optimized by monitoring the formation of Au_2O_3 on pure Au substrates.[40] It should also be noted that XPS analysis of the SAMs used in this study revealed that oxygen was the only new element detected during exposure to AO. This was taken as evidence for the chemical purity of the AO generated from the thermal gas cracker. During experiments, surfaces are exposed to a mixture of AO and molecular oxygen $(O(^3P)/O_2)$. The absence of reactivity, evidenced by the invariant C(1*s*) signal and the absence of any intensity in the O(1*s*) XPS region for any of the SAMs following exposure to either (a) molecular oxygen dosed onto the SAMs through the radical source at similar pressures and exposure times reported in the present study but with the source held at room temperature; or (b) the radical source heated to the same conditions used to generate AO (45 W), but in the absence of molecular oxygen for a period of several hours, indicates that all of the reactions reported in this investigation are initiated by AO.

III. RESULTS

A. Effect of AO exposure on CF-SAMs

Figure 1 shows the evolution of the F(1*s*), O(1*s*), C(1*s*) and S(2*p*) XP spectral regions for separately prepared semifluorinated self-assembled monolayers (CF-SAMs) as a function of increasing exposure time to AO. Figure 2 shows the variation in the O(1*s*), S(2*p*), and Au(4*f*) XPS areas, while Fig. 3 shows the corresponding variation in the C(1*s*) and F(1*s*) XPS areas as well as the C(1*s*)/F(1*s*) ratio. It should be noted that the S(2*p*), Au(4*f*), C(1*s*), F(1*s*) XPS areas and the C(1*s*)/F(1*s*) elemental ratios have been nor-

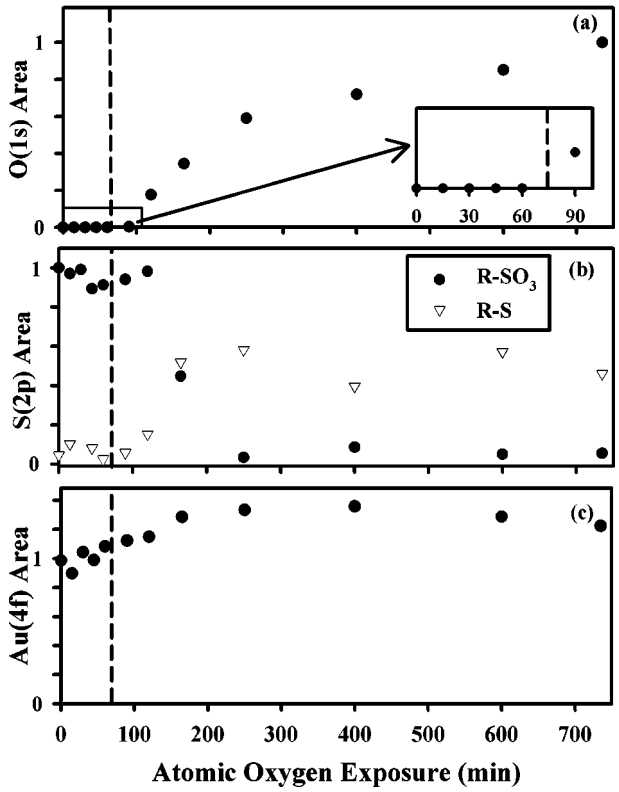

FIG. 2. Variation in (a) the O(1*s*) XPS area, (b) the thiolate (R–S—inverted open triangles) and sulphonate (RSO_3—filled circles) areas in the S(2*p*) region, and (c) the Au(4*f*) XPS area as a function of AO exposure. The insert in (a) displays an expanded region of the oxygen O(1*s*) XPS area illustrating the onset of oxygen uptake. The onset of oxygen uptake in the film is shown explicitly as a dashed line in (a)–(c).

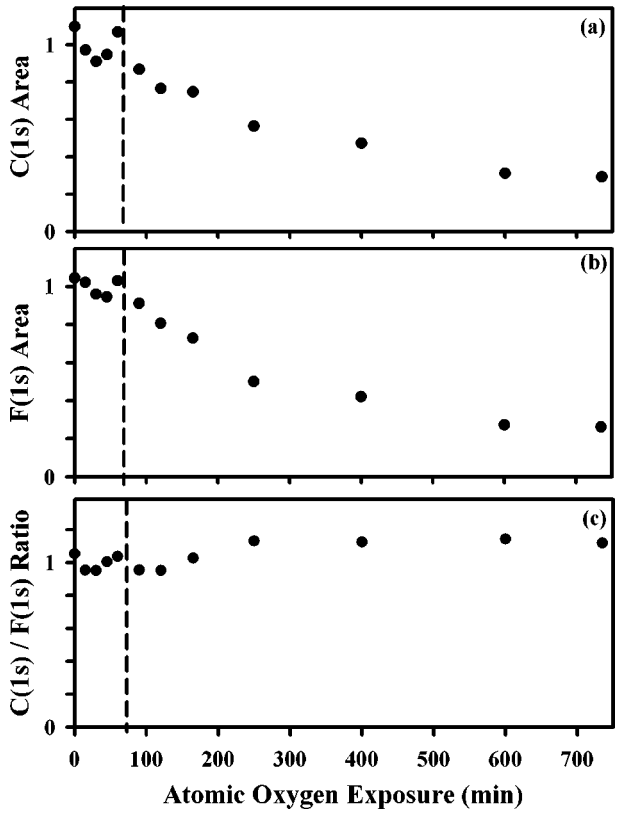

FIG. 3. Variation in (a) the integrated C(1*s*) XPS area, (b) the integrated F(1*s*) XPS area, and (c) the C(1*s*)/F(1*s*) XPS ratio as a function of AO exposure time. The dashed line in (a)–(c) indicates the AO exposure at which O(1*s*) intensity is observed.

malized to the pristine CF-SAM, while the O(1*s*) XPS area has been normalized to the O(1*s*) XPS area observed after 720 min of AO exposure to the CF-SAM. Thus, the data shown in Figs. 2 and 3 provides a measure of relative changes within the film's chemical composition.

Figure 1(a) shows the XP spectra of a native CF-SAM film before exposure to AO. The F(1*s*) region in Fig. 1(a) exhibits a single peak assigned to fluorine bound to carbon (C–F), centered at ≈688 eV, while the C(1*s*) region contains three distinct peaks due to the CF_3 (292.8 eV), CF_2 (290.2 eV), and C–H/C–C (284.5 eV) species, and the S(2*p*) region contains a $2p_{3/2}/2p_{1/2}$ doublet ($2p_{3/2}$ = 161.8 eV) consistent with the formation of a gold–thiolate (R–S–Au) bond.[48] No spectral intensity is observed in the O(1*s*) region. The XP spectra shown in Fig. 1(a) are consistent with published XP spectra of $CF_3(CF_2)_7(CH_2)_2SH$ adsorbed on Au.[42,49,50] Furthermore, the absence of intensity in the C(1*s*) region between the CF_2 peak at 290.2 eV and the C–H/C–C peak at 284.5 eV indicates that the x-ray exposure necessary to acquire the XP spectra shown in Fig. 1(a) does not itself produce any changes to the film's chemical composition, notably the production of CF groups.[38,42,50]

For CF-SAMs exposed to AO for 15, 30, 45, and 60 min there were no detectable changes in the chemical composition of the film or the gold substrate, as detected by XPS. Thus, the F(1*s*), O(1*s*), C(1*s*), and S(2*p*) XPS areas remain unchanged compared to the native CF-SAM. For an AO exposure of 90 min, however, Fig. 1(c) shows that a small peak appears at ≈530.2 eV in the O(1*s*) region [shown explicitly in the insert in Fig. 2(a)]. The dashed line drawn in Figs. 2 and 3 indicates the duration of the induction period (≈75 min), during which time the CF-SAM remains intact and the film is chemically unaltered.

The new peak observed in the O(1*s*) region (530.2 eV) after 90 min of AO exposure coincides with that observed during exposure of clean Au substrates to AO, and is ascribed to the formation of Au–O bonds associated with Au_2O_3.[51–53] This assignment is also consistent with a slight broadening observed in the Au(4*f*) XPS profile to higher binding energies (not shown) due to the presence of oxidized Au atoms.[40,53] However, due to the presence of a large background signal associated with the gold substrate coupled with the fact that the overall gold intensity changes during exposure to AO (due to the film's erosion) the production of Au_2O_3 is most clearly evidenced by the appearance and peak position of the O(1*s*) signal. In this context it should be noted that the O(1*s*) peak position [and slight broadening of the Au(4*f*) signal to higher binding energies] associated with Au_2O_3 production was calibrated by exposure of AO to a pure gold substrate as shown in Fig. 1 of Ref. 40.

The appearance of oxygen for AO exposures >90 min coincides with the onset of fluorine and carbon loss from the film, measured by the C(1*s*) and F(1*s*) peak areas (Fig. 3). Although the total carbon content in the film decreases steadily for AO exposures >90 min (Fig. 3), Fig. 1 shows

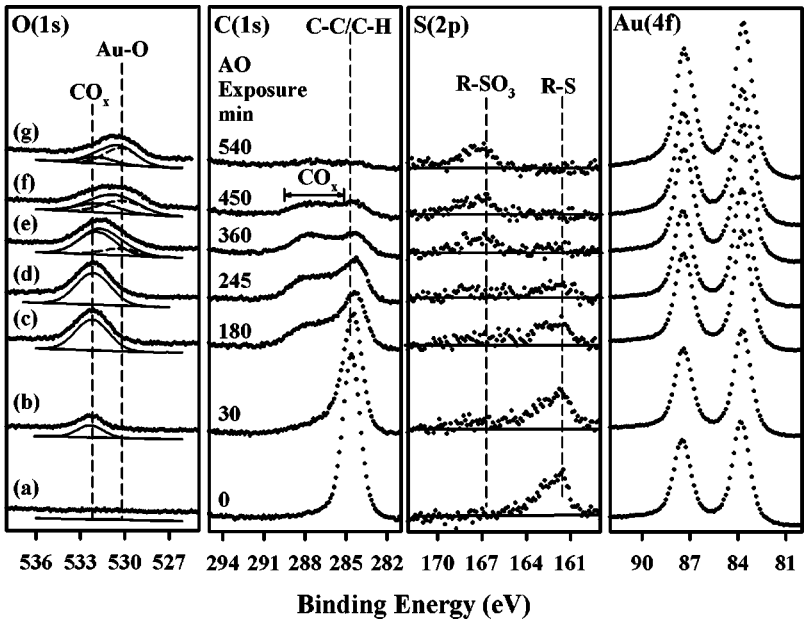

FIG. 4. Variation in the O(1*s*), C(1*s*), S(2*p*), and Au(4*f*) XPS regions of a C_{16}-SAM as a function of AO exposure time; (a) 0 min, (b) 30 min, (c) 180 min, (d) 245 min, (e) 360 min, (f) 450 min, and (g) 540 min. The XPS peaks associated with the native C_{16}-SAM are the C–C/C–H C(1*s*) peak at 284.5 eV and the thiolate (R–S–Au) species [S($2p_{3/2}$) peak at 161.8 eV]. The product species observed in XPS due to the interaction of AO with the C_{16}-SAM are oxygen-containing carbon functionality (CO_x species) observed at 532.8 eV in the O(1*s*) region and between 286–290 eV in the C(1*s*) region, Au_2O_3 centered at 530.2 eV in the O(1*s*) region, and sulphonate ($R–SO_3$) species [S($2p_{3/2}$) peak at 166.9 eV]. The peak fits in the O(1*s*) region have been offset for clarity. Each XP spectra shown in Fig. 4 corresponds to results obtained on a separately prepared C_{16}-SAM that was analyzed by XPS only after AO exposure.

that the C(1*s*) spectral envelope remains qualitatively unchanged from that of the native CF-SAM. For example, the C(1*s*) spectral envelopes in Figs. 1(a) and 1(e) are comparable, although the integrated C(1*s*) XPS area in Fig. 1(e) has decreased to 68% of the value associated with the native CF-SAM. It should be noted, however, that the loss in CF_3, CF_2 and C–C/C–H peaks is accompanied by the appearance of a small amount of new spectral intensity between the CF_2 peak at 290.2 eV and the C–C/C–H peak at 284.5 eV. The assignment of this new component is discussed in Sec. IV. The F(1*s*) XPS area exhibits a similar variation to that of the integrated C(1*s*) XPS area, remaining constant for AO exposures <90 min but decreasing at longer exposure times. Indeed, Fig. 3 shows that despite the loss of fluorine and carbon from the film, the C(1*s*)/F(1*s*) ratio [shown in Fig. 3(c)] remains virtually constant for all AO exposures.

During the initial period of AO exposure, the only sulfur-containing species observed in the S(2*p*) region are the gold–thiolate (R–S–Au) sulfur atoms associated with the native CF-SAM observed between 165–160 eV. However, Figs. 1(d)–1(g) and Fig. 2 show that after 120 min of AO exposure the S(2*p*) region broadens noticeably to higher binding energies and after an AO exposure of 165 min a new component can be resolved between ≈166.5–169 eV. This new spectral feature can be identified with the production of a sulfonate ($R–SO_3$) species ($2p_{3/2}$ peak at ≈167.0 eV).[39,54–56] The S(2*p*) XPS area of these two sulfur-containing species (R–S and $R–SO_3$) as a function of AO exposure are plotted in Fig. 2(b). This analysis shows that once sulfonate species have been produced, their relative intensity increases at the expense of the native thiolate species. Thus, for AO exposure times >120 min, the $R–SO_3$ species become the exclusive sulfur-containing species in the film (Fig. 2).[57]

The Au(4*f*) XPS peak area (XPS data not shown) shows a modest increase during AO exposure [Fig. 2(c)]. Thus, after 400 min of AO exposure, the Au(4*f*) peak area has increased by ≈30%, indicating that reactions of AO with the CF-SAM lead to erosion of the film and a consequent increase in the intensity of the detected Au(4*f*) photoelectrons.

B. Effect of AO exposure on *n*-alkanethiolate SAMs

Figure 4 shows the evolution of the O(1*s*), C(1*s*), S(2*p*), and Au(4*f*) XPS regions of C_{16}-SAMs as a function of increasing AO exposure. Prior to AO exposure [Fig. 4(a)], the C_{16}-SAM exhibits no intensity in the O(1*s*) region, a single peak in the C(1*s*) region centered at 284.5 eV (corresponding to the $C–C/CH_2/CH_3$ species), a R–S ($2p_{3/2}$:$2p_{1/2}$) doublet with the $2p_{3/2}$ peak at 161.8 eV and a Au ($4f_{7/2}$:$4f_{5/2}$) doublet with the $4f_{7/2}$ peak centered at 83.8 eV.[58] After 30 min of AO exposure Figure 4(b) shows that a peak at 532.8 eV is observed in the O(1*s*) region, indicative of the incorporation of carbon-containing oxygen functional groups (C–O, C═O and O–C═O—hereafter referred to as CO_x species) into the film.[39] As a result of the production of these CO_x species, the C(1*s*) region broadens to higher binding energies.[36] Following 180 min of AO exposure [Fig. 4(c)], changes in the O(1*s*) and C(1*s*) XP spectral regions indicate that the concentration of carbon-containing oxygen functionality in the film has increased, while the concentration of C–C and C–H bound species [measured by the intensity of the C(1*s*) peak at 284.5 eV] has decreased. A comparison of the integrated area of the C(1*s*) spectral envelopes in Figs. 4(a) and 4(c) also points to the overall loss of carbon from the film that accompanies exposure of the C_{16}-SAM to AO. Despite the loss of carbon from the film, an analysis of the S(2*p*), Au(4*f*), and O(1*s*) regions indicates that after 180 min of AO exposure, no chemical transformations have occurred to either the sulfur atoms located at the film/substrate interface or to the Au substrate itself, the latter evidenced by the absence of any Au–O species in the O(1*s*) region.

For C_{16}-SAMs exposed to AO between 180 and 300 min, the concentration of carbon-containing oxygen func-

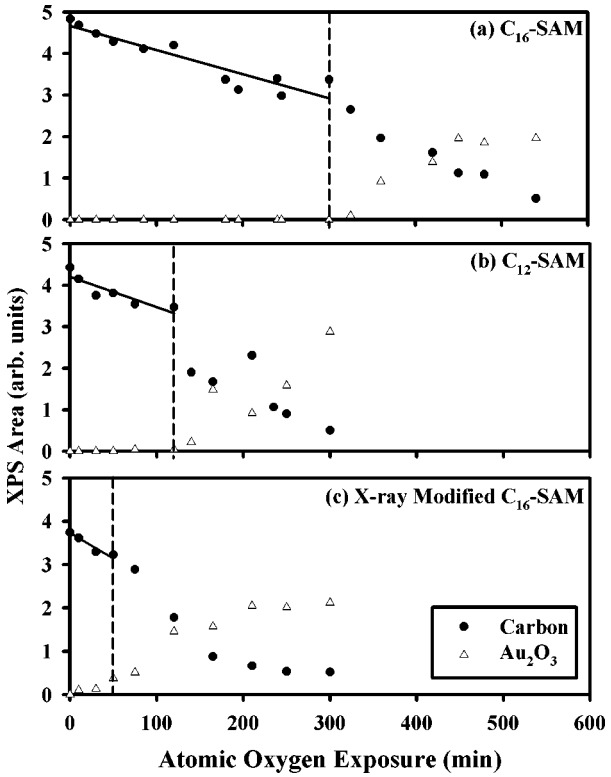

FIG. 5. Variation in the integrated C(1*s*) XPS area (●) and the Au_2O_3 concentration (▽) [the latter determined from deconvolution of the O(1*s*) region] as a function of AO exposure time for (a) C_{16}-SAMs, (b) C_{12}-SAMs, and (c) an x-ray modified C_{16}-SAM. The solid lines represent the best-fit values corresponding to zeroth-order kinetics for carbon loss from the film (see the text for details). The dashed line represents the AO exposure at which reactivity is observed at the film/substrate interface, evidenced by the appearance of Au_2O_3.

tionality remains virtually constant. This is supported experimentally by the fact that for this time period the area of the higher binding energy shoulder in the C(1*s*) XPS region (Fig. 4) assigned to CO_x species and the O(1*s*) peak area [measured from the C(1*s*) region] remain virtually unchanged. The total carbon content [monitored by the integrated area within the C(1*s*) region], however, continues to decrease over this same time interval [Fig. 5(a)], due to a loss of C–C/C–H carbon atoms [cf. the C(1*s*) regions in Figs. 4(c) and 4(d)].

For AO exposures ⩾300 mins (Fig. 4), AO penetrates to the film/substrate interface, evidenced by the appearance of sulfonate ($R–SO_3$) species in the S(2*p*) region[39,55,56] ($2p_{3/2}$ peak centered at ≈167 eV) and the broadening of the O(1*s*) spectral envelope to lower binding energies due to the production of Au_2O_3 species (the peak centered at ≈530.2 eV).[51–53] Analogous to the results obtained on the CF-SAM (Figs. 1 and 2), once the $R–SO_3$ species are produced, their relative concentration increases rapidly, such that for AO exposures >300 min they are the dominant sulfur-containing species within the film. Similarly, over this same time period the Au_2O_3 signal continues to increase, evidenced by the evolution of the O(1*s*) XPS peak at 530.2 eV (Fig. 4). The continued loss of carbon from the film (erosion) for these extended AO exposures is indicated by the loss of XPS intensity within the C(1*s*) region (Figs. 4 and 5), the reduction in the concentration of CO_x species observed in the O(1*s*) region and a corresponding increase in the Au(4*f*) intensity (Fig. 4). Ultimately, for a C_{16}-SAM exposed to AO for 540 min there is no discernable carbon left in the film, and the surface is composed exclusively of sulfonate species and Au_2O_3 [Fig. 4(g)].

Figure 5 shows the variation in the total carbon content [determined from the integrated area of the C(1*s*) XPS profile] and Au_2O_3 concentration as a function of AO exposure to (a) a C_{16}-SAM, (b) a C_{12}-SAM, and (c) an x-ray modified C_{16}-SAM. The variation in the carbon content among the three films exhibit qualitative similarities, with two distinct regimes. For each film, the carbon content in the film initially decreases linearly with increasing exposure to AO. At the point where Au_2O_3 is observed (shown as a dashed line in Fig. 5), however, the rate at which carbon is lost from the films as a function of AO exposure increases. For each of the three hydrocarbon films studied the linear decrease in the carbon content during the initial stages of AO-induced reactivity, corresponding to zeroth-order kinetics, are shown as solid lines. Figure 5 reveals that although the qualitative variation in carbon content of the three films is similar, the time scales for the reaction kinetics vary considerably.

IV. DISCUSSION

A. Reactivity of the CF-SAM with AO

1. Initial period of AO exposure

Figures 1–3 reveal that, for short AO exposures, the CF-SAM is chemically unreactive toward AO. This assertion is supported by the absence of any measurable change in the XPS areas within the C(1*s*), F(1*s*), or S(2*p*) regions compared to the pristine CF-SAM, coupled with the absence of oxygen uptake. The initial inertness of the CF-SAM toward reactions with AO can be ascribed in part to the close-packed, well-ordered molecular film that is formed during the reaction of the $CF_3(CF_2)_7(CH_2)_2SH$ adsorbate with Au.[42,59] As a result of the well-ordered nature of the film, permeation of AO to the underlying Au substrate is hindered. This initial period of chemical inertness is indicated by the vertical dashed line in Figs. 1–3. In addition to the physical characteristics of the film, the lack of initial chemical reactivity between AO and the CF-SAM indicates that the $O(^3P)$ atoms generated by thermal dissociation in the atom source (E_{kin}≈0.11 eV) are unable to activate either C–F or C–C bond cleavage within the CF-SAM, shown schematically in Fig. 6(a). A similar example of an induction time in the reactions of ordered SAMs has been observed in atmospheric oxidation studies of *n*-alkanethiolates adsorbed on copper, where for $CH_3(CH_2)_{17}SH$ and $CH_3(CH_2)_{21}SH$ adsorbates no evidence of oxidation was detected for atmospheric exposures <100 h.[55] This effect was ascribed to the lack of chemical reactivity between O_2 and the C–H and C–C bonds of the alkanethiolate monolayer coupled with the well-ordered and densely packed nature of the SAM. Figure 1 also suggest that although there is no measurable change in the area of the S(2*p*) peak during this induction time, the thiolate peak is broader than that observed for the native CF-SAM prior to AO exposure (Fig. 1). A similar phenomenon

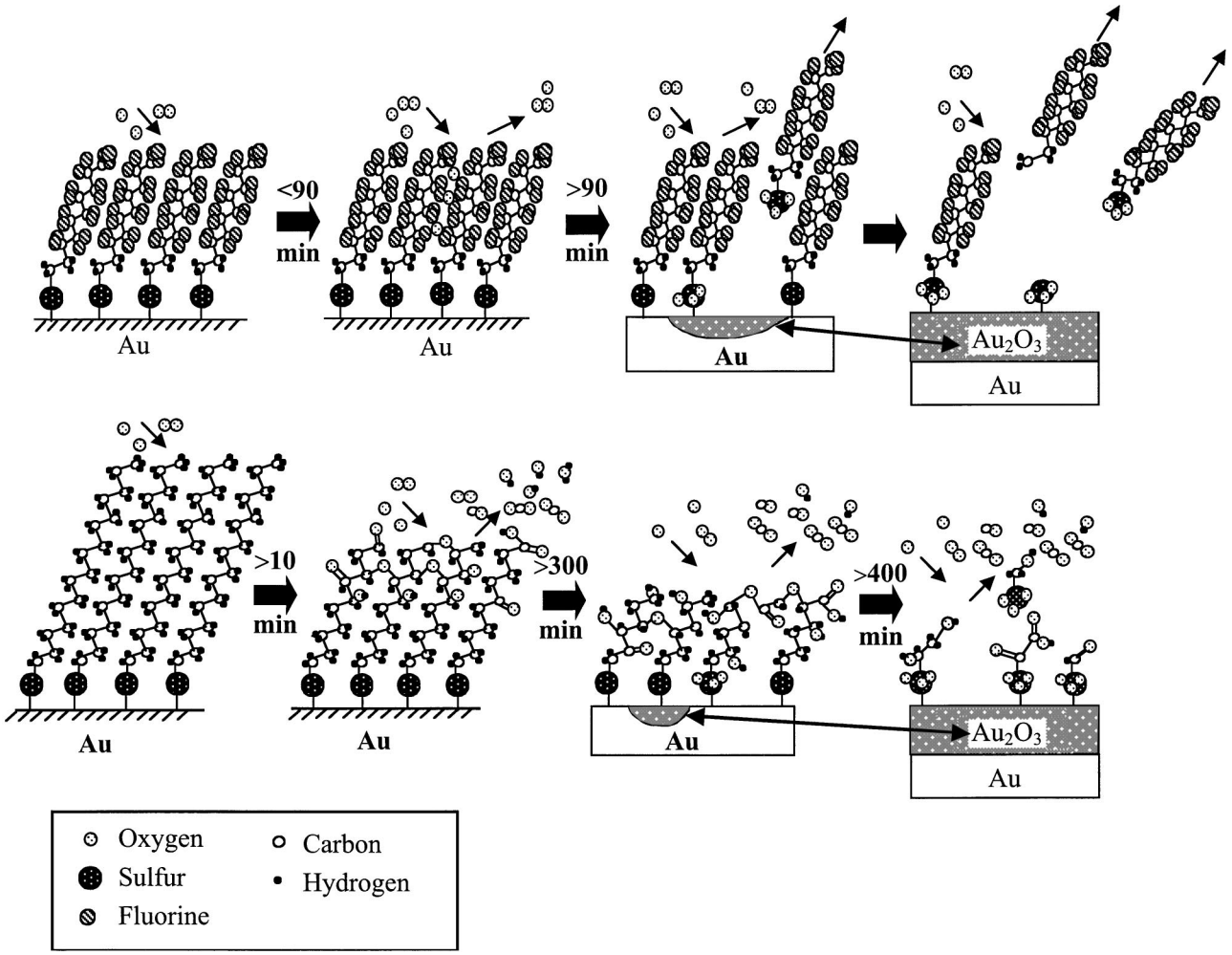

FIG. 6. A schematic depiction of atomic oxygen reactions with (a) CF-SAMs and (b) C_{16}-SAMs. The various stages of reactivity are depicted for both films following specified AO exposures.

was also observed during AO exposure to alkanethiolate SAMs (Fig. 4). The reason for this peak broadening is unclear but may reflect an increase in structural disorder within the CF-SAM due to AO exposure. In this context it should be noted that a broader S($2p$) region has been observed in XPS studies of *n*-alkanethiols adsorbed on polycrystalline Cu substrates[41,58] and has been ascribed to a more heterogeneous bonding environment at the film/substrate interface. Any increase in the structural disorder within the CF-SAM is also likely to increase the permeability of AO through the film.

2. Reactivity of AO at the substrate/film interface

Reactivity within the CF-SAM is initiated by the permeation of AO through the uppermost portion of the CF-SAM, which contains exclusively C–F and C–C bonds, to the film/substrate interface. The permeation of AO to the film/substrate interface is accompanied by the onset of chemical reactivity within the film, evidenced by the appearance of sulfonate ($R–SO_3$) species and Au_2O_3 [Figs. 1 and 3(b)]. Although the detailed mechanism responsible for the migration of the reactive species (AO) through the CF-SAMs cannot be determined unambiguously from XPS studies alone, it is reasonable to assume that O atom permeation and subsequent reactivity is at least initiated in proximity to defect sites (e.g., domain boundaries) within the SAM rather than uniformly throughout the film. This assertion is also consistent with proposed mechanisms for oxygen transport studies through lipid bilayers[60] and alkanethiolate SAMs.[55] The overall defect density within the CF-SAM is also expected to be influenced by the nature of the Au substrates. In the present investigation polycrystalline gold substrates were employed. Although the CF-SAMs formed on these substrates produces a densely packed overlayer, the defect density in these films (at grain boundaries, for example) is likely to be reduced on more well-ordered single crystal Au(111) substrates. As a result, the duration of the induction period observed in the present study may well increase for CF-SAMs adsorbed on Au(111).

Once chemical reactivity is initiated at the film/substrate interface, the desorption of carbon and fluorine from the CF-SAM is observed (Figs. 1 and 3). Furthermore, a comparison of Figs. 2 and 3 demonstrates that oxygen uptake is correlated with the loss of both fluorine and carbon from the film. This supports the idea that carbon and fluorine desorption from the CF-SAM is initiated by reactions of AO at the film/substrate interface. Despite the desorption of both car-

bon and fluorine from the film, however, the C/F ratio remains essentially invariant throughout the course of the reaction [Fig. 3(c)], indicating that carbon and fluorine are being lost at an equal rate.

Figure 1 also shows that during exposure to AO the C(1*s*) spectral envelope remains essentially unchanged from that of the native CF-SAM, despite the desorption of fluorine and carbon from the film. For example, analysis of the normalized C(1*s*) spectra shown in Fig. 1 reveals that the CF_3:CF_2:CH_2 ratio remains virtually unchanged from that of the pristine CF-SAM for all but the longest AO exposures. Taken in conjunction with the nearly constant C/F ratio observed during AO exposures to the CF-SAM, these results strongly suggest that the desorption of carbon and fluorine from the film is dominated by the loss of fragments that incorporate intact adsorbate chains. These volatile species that contain intact adsorbate chains are postulated to result from AO-induced carbon–sulfur and sulfur–gold bond cleavage processes, initiated by AO reactions at the film/substrate interface. Thus, the chemical identity of these volatile species are postulated to include fragments such as $CF_3(CF_2)_7(CH_2)_2$ and $CF_3(CF_2)_7(CH_2)_2SO_3$, as shown in Fig. 6.

3. Secondary processes

An analysis of the C(1*s*) envelope in Fig. 1 reveals that once the AO-induced desorption of fluorine and carbon from the CF-SAM is initiated, a small amount of additional intensity appears in the C(1*s*) spectral envelope between the CF_2 peak at ≈290.2 eV and the hydrocarbon C–C/C–H peak at ≈284.5 eV. This additional intensity is postulated to arise in part from reactions between AO and the native CH_2 species proximate to the film/substrate interface,[40] which lead to the formation of carbon-containing oxygen functional groups (C–O, C═O, and O–C═O) still bound to the Au substrate. In addition, we propose that the new XPS intensity observed in the C(1*s*) region between the CF_2 and C–C/C–H peaks is a reflection of the CF species produced from secondary C–F bond cleavage reactions between volatile carbon-containing radicals [e.g., $CF_3(CF_2)_7–CH_2–\cdot CH_2$] liberated by AO reactions at the film/substrate interface and CF_2 groups associated with $CF_3(CF_2)_7(CH_2)_2S$ adsorbate species still tethered to the Au substrate, that occur as the carbon-containing radicals escape (desorb) from the film. Experimental evidence for C–F bond cleavage from reactions involving carbon-containing radicals such as $CF_3(CF_2)_7–CH_2–\cdot CH_2$ can be found in recent tandem mass spectrometry experiments by Cooks and co-workers, who observed the formation of $FCH_2OCH_2^+$ during the interaction of the radical $\cdot CH_2OCH_2^+$ ion at low incident kinetic energy (18 eV) with semifluorinated SAM surfaces.[61] In contrast, reactions of the closed-shell methoxymethyl cation $CH_3OCH_2^+$ with the same surface, also at low collision energies, did not produce any fluorine-containing species, indicating that C–F bond activation is associated with reactions involving the carbon-containing radical.[61]

We also postulate that AO reactions with the $CH_2–CH_2$ group proximate to the film/substrate interface leads to C–C bond cleavage and the ejection of a small number of fragments such as $CF_3(CF_2)_7\cdot CH_2$ that are ''carbon deficient'' compared to those that contain intact adsorbate chains [e.g., $CF_3(CF_2)_7(CH_2)_2SO_3$]. Indeed, both the loss of the ''carbon deficient'' species such as $CF_3(CF_2)_7\cdot CH_2$ and the loss of fluorine from C–F bond cleavage during collisions between carbon-based radicals such as $CF_3(CF_2)_7\cdot CH_2$ and CF_2 groups within the adsorbate structure will increase the C/F XPS ratio, consistent with the slight increase in the film's C/F XPS ratio following prolonged AO exposures (>250 min). It should be emphasized, however, that compared to the loss of entire adsorbate chains due to AO-induced C–S and Au–S bond cleavage, these processes represent a minor secondary reaction pathway. Thus, even after 720 min of AO exposure to the CF-SAM, the XPS intensity in the C(1*s*) region between 290.2 and 284.5 eV is less than 10% of the total original C(1*s*) area for the native CF-SAM (Fig. 1—bottom spectra). Similarly, the slight increase in the C/F XPS ratio is only a minor perturbation compared to the total amount of carbon and fluorine lost from the film during exposure to AO. Indeed, the nearly constant C/F XPS ratio observed in this study suggests that AO reactions with the adsorbate chain are dominated by C–S and/or Au–S bond cleavage events, leading to the desorption of intact adsorbate chains, rather than C–C bond cleavage due to AO reactivity with the $CH_2–CH_2$ linkage, which would produce a volatile ''carbon-deficient'' species and a more significant increase in the C/F XPS ratio than is observed experimentally.

4. Fate of sulfur

In contrast to fluorine and carbon, the fate of sulfur during reactions with AO appears to involve a competition between oxidation, producing a sulfonate species [evidenced by the evolution of the S(2*p*) region shown in Fig. 1], and oxidation coupled with the desorption of RSO_3 species [e.g., $CF_3(CF_2)_7(CH_2)_2SO_3$]. In the present study sulfur desorption is implicated by the decrease in the S(2*p*) XPS area during exposure to AO, despite the loss of both fluorine and carbon from the film. If sulfur desorption did not occur during AO exposure, the loss of carbon and fluorine would produce an increase in the S(2*p*) XPS area, in contrast to our experimental observations. Furthermore, the S(2*p*):C(1*s*) XPS ratio (calculated from the data contained in Figs. 2 and 3) remains relatively constant for all but the longest AO exposures, consistent with the idea that sulfur and carbon desorption from the film are correlated. In this context desorption of RSO_3 species has also been identified in the UV photo-oxidation of alkanethiolate SAMs, where a decrease in the S(2*p*) area was observed despite the loss of carbon.[62] However, not all of the sulfur atoms at the film/vacuum interface desorb. This is evidenced most clearly in the present investigation by the continued presence of bound sulfonate species during AO reactions with the C_{16}-SAM (Fig. 4) despite the loss of virtually the entire carbon content of the film. The fact that this competition between desorption and oxidation is observed for both the CF-SAM and the alkanethiolate SAMs is probably a reflection of the similar chemical bonding environment of the initial thiolate sulfur atoms (R–S–Au) in both systems.

5. Influence of chemical and structural characteristics on AO reactivity

In the CF-SAMs, initial reactivity induced by exposure to AO is controlled by the permeation of oxygen atoms to the film/substrate interface due the chemical inertness of both C–F and C–C bonds. The role of structural integrity within the CF-SAMs is also likely to play a role in the overall reaction time scale. This idea is supported by results obtained in related experiments carried out as part of this investigation, where CF-SAMs exposed to a dose of x-ray irradiation insufficient to produce any change in the C(1*s*) profile still exhibited a marked increase in their reactivity (and degradation) during subsequent exposure to AO compared to CF-SAMs that were not exposed to any x rays prior to AO exposure.

B. Reactivity of alkanethiolate SAMs with AO

The interaction of AO with the alkanethiolate SAMs (including the x-ray modified C_{16}-SAM) also leads to the production of Au_2O_3 and RSO_3 species as well as erosion of the organic film. However, the detailed molecular level events associated with the interaction of AO with CF-SAMs and the alkanethiolate SAMs studied in this investigation differ significantly. In the following discussion we shall focus on the reactivity of AO with the C_{16}-SAM before comparing these results with those obtained on the C_{12}-SAM and the x-ray modified hydrocarbon film (derived from the C_{16}-SAM).

1. AO reactivity with C_{16}-SAMs

In contrast to the CF-SAM, AO reactions with the three hydrocarbon films are initiated by $O(^3P)$-mediated H atom abstraction from the C–H bonds at the vacuum/film interface and the subsequent formation of carbon-containing oxygen (CO_x) functional groups.[40] Experimentally determined activation energies for hydrogen abstraction from saturated hydrocarbons typically lie in the range 14–30 kJ mol^{-1}, compared to theoretically determined values of >150 kJ mol^{-1} for C–C bond cleavage.[63,64] Thus, it is clear that $O(^3P)$ interactions with hydrocarbons are dominated by H atom abstraction from C–H bonds,[65] followed by the reaction of atomic and molecular oxygen with the resultant alkyl radicals.[20,40] This can be represented schematically, thus

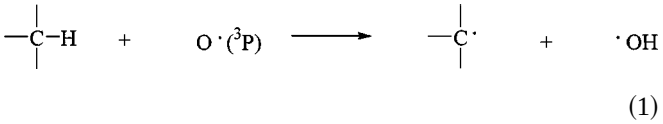

(1)

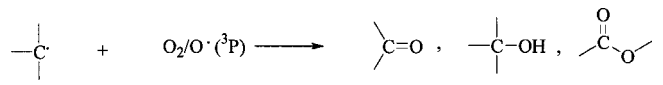

(2)

In the case of the C_{16}-SAM, the production of these carbon-containing oxygen functional groups is evidenced by the appearance of an O(1*s*) peak at ≈532.1 eV and the broadening of the C(1*s*) spectral envelope to higher binding energies (Fig. 4). The fact that AO reactions in the three hydrocarbon films are restricted to the vacuum/film interface is a reflection of the limited penetration depth of AO in these films.[46] This is observed experimentally by the absence of oxidation for sulfur atoms located at the film/substrate interface during the initial stages of AO-induced reactions, despite significant chemical transformations within the hydrocarbon film. In contrast, reactivity within the CF-SAM is initiated by AO reactions at the film/substrate interface due to the inertness of C–C and C–F bonds toward the thermalized AO employed in this investigation. These differences are illustrated schematically in Fig. 6.

2. Carbon desorption kinetics

Figure 5 shows that the C(1*s*) XPS area decreases linearly during the initial stages of AO reactions for all three of the hydrocarbon films studied in this investigation. Despite this decrease in the C(1*s*) XPS area, however, the Au(4*f*) XPS area remains virtually unchanged. For example, a comparison of the Au(4*f*) spectra shown in Figs. 4(a) and 4(c) reveals that the intensity of the Au(4*f*) transitions and the integrated XPS intensity within the Au(4*f*) region are nearly identical, despite significant changes in the chemical composition and carbon content of the film. This indicates that the decrease in the C(1*s*) signal is dominated by the loss of carbon from the film rather than any change in the effective escape depth of the C(1*s*) photoelectrons due to the incorporation of oxygen into the film.

Carbon desorption from the film is a result of the formation of volatile carbon-containing species, notably CO and CO_2, produced during AO reactions with the CO_x species in the hydrocarbon films.[22,24,40] As carbon is lost, underlying hydrocarbon layers are exposed at the vacuum/film interface. Subsequent AO reactions with these newly exposed carbon atoms sustains the erosion and leads to the creation of an etch front. This etch front is responsible for the decrease in the total carbon content of the two alkanethiolate SAMs and the x-ray modified C_{16}-SAM studied in this investigation. The fact that the overall thickness of the film, measured by the Au(4*f*) XPS area, does not change significantly during the initial stages of AO reactions can be ascribed to the balance between carbon desorption and oxygen incorporation into the film.

Since the flux of oxygen atoms generated by the atom source is constant under our experimental conditions, the initially linear decrease in carbon content (shown in Fig. 5) is consistent with zeroth-order kinetics, indicative of a constant rate of carbon desorption that is independent of the carbon content/thickness of the film. This kinetic dependence has been explained by the fact that, in this linear regime, the concentration of carbon-containing species that can react with impinging oxygen atoms (and subsequently desorb due to the formation of CO and CO_2) is constant, due to the limited penetration depth of oxygen atoms within the hydrocarbon films.[40] Ultimately, under these conditions a steady-state etch front is produced. This is denoted by an AO exposure interval for which a nearly constant O(1*s*) XPS area is observed, despite the fact that the total carbon content in the film continues to decrease. In the case of the C_{16}-SAM, this is observed between ≈180–320 min of exposure to AO (Fig. 4), illustrated schematically in Fig. 6. Corresponding changes to the C(1*s*) region during this stage of the reaction

[compare Figs. 4(c), 4(d), and 4(e)] indicate that the concentration of CO_x species remains essentially unchanged, while the concentration of C–C/C–H species decreases, consistent with the production of a steady-state etch front.

For prolonged O atom exposures, a point is reached when the rate of carbon loss from the film increases. In Fig. 5 the approximate AO exposure that corresponds to this change in the carbon desorption kinetics is represented by a dashed line for the C_{16}-SAM, the C_{12}-SAM and the x-ray modified C_{16}-SAM. An analysis of Fig. 5 shows that this AO exposure also corresponds closely to the exposure for which significant oxygen reactivity is observed at the film/substrate interface, evidenced by the production of Au_2O_3 in the O(1*s*) region and the appearance of a sulfonate ($R-SO_3$) species in the S(2*p*) region. This onset of AO reactivity at the film/substrate interface is also correlated with a rapid decrease in the concentration of oxygen-containing carbon (CO_x) species. This change in the carbon desorption kinetics is attributed to the fact that once AO is able to penetrate through to the film/substrate interface, the concentration of carbon available to react (and subsequently desorb) with incident oxygen atoms becomes limited by the film's thickness. As a result, the rate of carbon lost from the film for AO exposures in excess of the dashed line initially increases.[46] It should be noted that although the carbon desorption kinetics are now influenced by the fact that film's thickness is smaller than the penetration depth of oxygen atoms within the film, the facility of AO-induced Au–S and C–S bond cleavage (as noted in the reactions of AO with the CF-SAM) may also contribute to an increase in the effective desorption rate of carbon-containing fragments in this time regime.

3. Comparing the AO reactivity with C_{16}-SAMs, C_{12}-SAMs, and the x-ray modified C_{16}-SAM

A comparison of Fig. 5 reveals that the C_{16}-SAM, the C_{12}-SAM, and the x-ray modified C_{16}-SAM experience qualitatively similar variations in their chemical composition during exposure to AO. For example, Figs. 5(a) and (b) reveal that the C_{16}-SAM and the C_{12}-SAM experience a similar rate of initial carbon loss. Furthermore, the residual carbon content in the C_{16}-SAM and the C_{12}-SAM at the point when oxygen atoms react with the underlying Au substrate (indicated by the dashed lines in Fig. 5) is also similar. Indeed, differences in the kinetics observed between the C_{16}-SAM and the C_{12}-SAM are simply a reflection of the greater film thickness in the C_{16}-SAM. Thus, the difference in AO exposure required for Au_2O_3 formation to occur in the C_{16}-SAM and C_{12}-SAM provides a convenient estimate of the carbon desorption rate, based on the difference in the film thickness of C_{16}-SAMs and C_{12}-SAMs adsorbed on Au ($\approx$3.5 Å).[66] Results from this analysis reveals that in these alkanethiolate SAMs the AO-induced carbon desorption rate under steady-state etch conditions is ≈ 0.02 Å min^{-1}.

Similar reaction dynamics are also postulated to be responsible for the AO reactions with the x-ray modified C_{16}-SAM. However, more rapid film erosion is observed in this film compared to either the C_{12}-SAM or the C_{16}-SAM [Fig. 5(c)]. Thus, although the C_{12}-SAM and the x-ray modified C_{16}-SAM initially possess a similar carbon content [measured by the integrated C(1*s*) XPS area], AO-induced reactions result in a more rapid erosion of the x-ray modified C_{16}-SAM [Fig. 5(c)]. This increased reactivity is believed to be a result of the potential for the rapid AO addition to carbon–carbon double bonds, formed during the x-ray modification process in the x-ray modified film,[12,67] coupled with the greater permeability of the structurally disordered x-ray modified C_{16}-SAM[44] toward AO. It should also be noted that variations in the chemical composition of the x-ray modified C_{16}-SAM during exposure to AO are similar to those reported in our previous investigation,[40] although in the present study a higher incident AO flux was employed. This was necessary to enable the AO reactions of the four different films studied in this investigation to be completed on an experimentally accessible time scale.

4. O atom reactions with fluoropolymers in LEO and during plasma processing

Reactions of AO with fluorine-containing organic thin films are of relevance to studies of polymer degradation in LEO, where fluoropolymers such as FEP are exposed to the effects of sustained O(^3P) exposure.[13,15,16] Our results indicate that for thermalized oxygen atoms, C–C and C–F bonds are not susceptible to AO-induced scission. Thus, the electronegativity of fluorine appears to preclude a direct O atom-mediated abstraction mechanism in C–F bonds, in contrast to the potential for hydrogen abstraction in C–H bonds. Similarly, direct AO-mediated C–C bond breaking does not appear to contribute to the observed reaction dynamics under our experimental conditions.

The inertness of C–C and C–F bonds toward AO is also consistent with a limited set of experiments carried out in our laboratory on poly(tetrafluorethylene) [PTFE, $(CF_2-CF_2)_n$].[68] Results from these experiments revealed that even after 510 min of exposure to AO, the O(1*s*) area measured by XPS was $<1\%$. Thus, during oxygen plasma treatments of fluorinated polymers such as PTFE,[69,70] oxygen incorporation does not appear to be a direct result of thermalized AO interactions with the substrate but is instead a consequence of secondary reactions between carbon-containing radicals (themselves generated, for example, by ionizing radiation or electrons) and either molecular or atomic oxygen.[42]

Although C–C and C–F bonds are themselves not directly susceptible to (thermalized) AO-induced scission, our results indicate that carbon and fluorine can desorb as a result of AO reactions initiated at other ''reactive centers'' within the material. In the present study, these include C–H and C–S bonds, whose reactions with AO can lead to C–C bond scission and the production of volatile species that include carbon and fluorine. For the case of a CH_2-CF_2 linkage this is illustrated below:

(3)

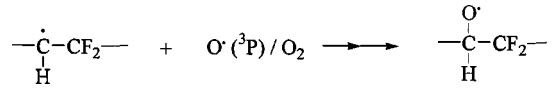

(4)

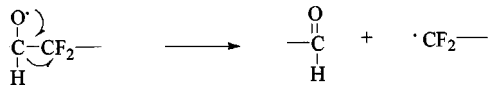

(5)

The existence of this degradation pathway is postulated to be at least in part responsible for the ejection of fragments that are "carbon deficient" [e.g., $CF_3(CF_2)_7(CH_2)$] compared to the intact adsorbate chains [fragments that include the $CF_3(CF_2)_7(CH_2)_2$ unit] for prolonged AO exposures to the CF-SAM. In the context of LEO studies, the existence of this degradation pathway is also consistent with the order of magnitude increase in the measured rate of mass loss for PVDF $(CF_2-CH_2)_n$ compared to PTFE under LEO conditions.[24,71]

5. Influence of hypethermal kinetic energies on O and O^+ reactivity

Under LEO conditions, oxygen-containing species strike the surface of an orbiting vehicle with a mean impact energy of $\approx$440 kJ mol^{-1} and an energy spread at full width half-maximum of $\approx$210 kJ mol^{-1}.[12,25,72] Indeed, recent theoretical studies have concluded that the additional relative kinetic energy associated with hyperthermal species could be sufficient to degrade fluorocarbons by direct $O(^3P)$ attack on C–C bonds,[32] in contrast to the observed inertness of C–F and C–C bonds toward thermalized $O(^3P)$ atoms in the present study. The interaction of hyperthermal AO and O^+ ions with fluorine-containing films may also lead to mechanistic differences in the degradation process due to the potential for C–F (BDE$\approx$5 eV) and/or C–C (BDE$\approx$3.6 eV) bond cleavage and the possibility of O^+ reactions at the vacuum/film rather than the film/substrate interface. In the case of the CF-SAM this would be evidenced experimentally in XPS by the appearance of CF groups and a C/F ratio that increases with AO or O^+ exposure.

6. Influence of the reactive medium on the degradation of CF-SAMs

The degradation/reactivity of fluorine-containing polymers is influenced by the nature of the reactive medium. In the case of the CF-SAM this is well illustrated by a comparison of the film's degradation pathways during exposure to ionizing radiation and AO. Thus, in the case of x-ray or electron beam irradiation of semifluorinated SAMs, the initial phase of the reaction is characterized by electron-stimulated bond breaking processes throughout the film, including Au–S, C–S, C–C, and C–F cleavage, leading to the desorption of intact adsorbate chains, alkyl fluoride radicals, and fluorine.[41,42,73] Carbon–carbon coupling reactions within the film during this initial phase of the reaction, however, lead to the production of a cross-linked carbonaceous overlayer that stabilizes the film toward further desorption, except for the continued loss of fluorine through electron stimulated C–F bond cleavage.[38,41] As a result of the continuous C–F bond cleavage during electron or x-ray mediated degradation of semifluorinated SAMs, the C/F ratio increases monotonically as a function of increasing x-ray or electron dose and CF moieties are produced as intermediates in the degradation process.[38,41,42,73] This is in contrast to the absence of direct C–F or C–C bond breaking processes observed in the present study during the interaction of AO with CF-SAMs, which proceeds via a more "selective" degradation process dominated by AO-mediated Au–S and C–S bond cleavage, leading to the desorption of adsorbate chains.

V. CONCLUSIONS

The reactions of thermalized atomic oxygen (E_{kin} $\approx$0.11 eV) with semifluorinated self-assembled monolayers adsorbed on Au are initiated by reactions at the film/substrate interface following the permeation of atomic O through the fluorine-containing overlayer. The reaction of atomic O at the film/substrate interface produces Au_2O_3 and RSO_3 species and the loss of fluorine and carbon, principally from the ejection of intact adsorbate chains. In contrast, O atom reactions with *n*-alkanethiolate SAMs and the x-ray modified *n*-alkanethiolate SAM are initiated at the film/vacuum interface, leading to the incorporation of oxygen-containing carbon functionality and the formation of an etch front that is responsible for the loss of carbon from the film.

ACKNOWLEDGMENTS

Support for this research was provided by a National Science Foundation CAREER award (#9985372) and a grant from the Petroleum Research Fund (PRF #35281-G5, G6) administered through the American Chemical Society. G.M.W. also acknowledges support from the Howard Hughes undergraduate summer research program administered through Johns Hopkins University. This work was carried out in the surface analysis laboratory at Johns Hopkins as part of the Materials Research Science and Engineering Center, funded through the National Science Foundation.

[1] H. F. Winters and J. W. Coburn, Surf. Sci. Rep. **14**, 161 (1992).
[2] M. L. Hitchman and K. F. Jensen, *Chemical Vapor Deposition: Principles and Applications* (Academic, San Diego, CA, 1993).
[3] M. Ikeda, H. Ito, M. Hiramatsu, M. Hori, and T. Goto, J. Appl. Phys. **82**, 4055 (1997).
[4] H. L. Duan, G. A. Zaharias, S. F. Bent, Thin Solid Films **395**, 36 (2001).
[5] "Panel on plasma processing of materials: Scientific opportunities and technological challenges," National Research Council, 1991.
[6] E. M. Liston, Adhesion **1989**, 199.
[7] C.-M. Chan, T.-M. Ko, and H. Hiraoka, Surf. Sci. Rep. **24**, 1 (1996).
[8] T. Engel, Surf. Sci. Rep. **18**, 91 (1993).
[9] S. A. Buntin and M. Litorja, J. Chem. Phys. **118**, 321 (2003).
[10] M. Litorja and S. A. Buntin, J. Vac. Sci. Technol. A **20**, 76 (2002).
[11] K. S. W. Champion, A. E. Cole, and A. J. Kantor, "Standard and reference atmospheres," Chap. 14; United States Air Force, Air Force Geophysics Laboratory, 1985.
[12] T. K. Minton and D. J. Garton, *Advanced Series in Physical Chemistry—Dynamics of Atomic-Oxygen-Induced Polymer Degradation in Low Earth Orbit (Chapter 9)* (World Scientific, River Edge, NJ, 2001), Vol. 11.
[13] I. L. Harris, A. R. Chambers, and G. T. Roberts, Mater. Lett. **31**, 321 (1997).
[14] R. C. Tennyson, Can. J. Phys. **69**, 1190 (1991).
[15] M. R. Reddy, J. Mater. Sci. **30**, 281 (1995).

[16] A. R. Chambers, I. L. Harris, and G. T. Roberts, Mater. Lett. **26**, 121 (1996).
[17] S. L. Koontz, K. Albyn, and L. J. Leger, J. Spacecr. Rockets **28**, 315 (1991).
[18] F. A. Rasoul, D. T. Hill, G. A. George, and J. H. O'Donnell, Polym. Adv. Technol. **9**, 24 (1998).
[19] M. A. Golub, T. Wydeven, and R. D. Cormia, Polymer **30**, 1571 (1989).
[20] M. A. Golub and R. D. Cormia, Polymer **30**, 1576 (1989).
[21] M. A. Golub, Makromol. Chem., Macromol. Symp. **53**, 379 (1992).
[22] T. K. Minton, J. Zhang, D. J. Garton, and J. W. Seale, High Perform. Polym. **12**, 27 (2000).
[23] J. Zhang and T. K. Minton, High Perform. Polym. **13**, S467 (2001).
[24] B. Cazaubon, A. Paillous, and J. Siffre, J. Spacecr. Rockets **35**, 797 (1998).
[25] E. Murad, Annu. Rev. Phys. Chem. **49**, 73 (1998).
[26] D. Smith and P. Spanel, Mass Spectrom. Rev. **14**, 255 (1995).
[27] J. Zhang, D. J. Garton, and T. K. Minton, J. Chem. Phys. **117**, 6239 (2002).
[28] D. J. Garton, T. K. Minton, M. Alagia, N. Balucani, P. Casavecchia, and G. G. Volpi, Faraday Discuss. **108**, 387 (1997).
[29] D. J. Garton, T. K. Minton, M. Alagia, N. Balucani, P. Casavecchia, and G. G. Volpi, J. Chem. Phys. **112**, 5975 (2002).
[30] H. Kinoshita, M. Umeno, M. Tagawa, and N. Ohmae, Surf. Sci. **440**, 49 (1999).
[31] A. Gindulyte, L. Massa, B. A. Banks, and S. K. Rutledge, J. Phys. Chem. A **104**, 9976 (2000).
[32] A. Gindulyte, L. Massa, B. A. Banks, and S. K. R. Miller, J. Phys. Chem. A **106**, 5463 (2002).
[33] S. R. Carlo, A. J. Wagner, and D. H. Fairbrother, J. Phys. Chem. B **104**, 6633 (2000).
[34] C. C. Perry, S. R. Carlo, A. J. Wagner, C. Vecitis, J. Torres, K. Kolegraff, and D. H. Fairbrother, in *ACS Symposium on Solid Surfaces and Thin Films*, edited by M. Soriaga (American Chemical Society, Washington, DC, 2002).
[35] F. M. Elms and G. A. George, Polym. Adv. Technol. **9**, 31 (1998).
[36] X. J. Dai, F. M. Elms, and G. A. George, J. Appl. Polym. Sci. **80**, 1461 (2001).
[37] X. Qin, T. Tzvetkov, and D. C. Jacobs, Nucl. Instrum. Methods **203**, 130 (2003).
[38] C. C. Perry, A. J. Wagner, and D. H. Fairbrother, Chem. Phys. **280**, 111 (2002).
[39] Y. Paz, S. Trakhtenberg, and R. Naaman, J. Phys. Chem. **98**, 13517 (1994).
[40] J. Torres, C. C. Perry, S. J. Bransfield, and D. H. Fairbrother, J. Phys. Chem. B **106**, 6265 (2002).
[41] A. J. Wagner, S. Carlo, C. Vecitis, and D. H. Fairbrother, Langmuir **18**, 1542 (2002).
[42] A. J. Wagner, K. Han, A. L. Vaught, and D. H. Fairbrother, J. Phys. Chem. B **104**, 3291 (2000).
[43] M. Wirde, U. Gelius, T. Dunbar, and D. L. Allara, Nucl. Instrum. Methods **131**, 245 (1997).
[44] M. Zharnikov, W. Geyer, A. Golzhauser, S. Frey, and M. Grunze, Phys. Chem. Chem. Phys. **1**, 3163 (1999).
[45] F. Clouet and M. K. Shi, J. Appl. Polym. Sci. **46**, 1955 (1992).
[46] J. Torres, C. C. Perry, D. H. Fairbrother, Surf. Sci. **543**, 75 (2003).
[47] G. Herzberg, *Spectra of Diatomic Molecules* (Van Nostrand, Princeton, NJ, 1967).
[48] D. G. Castner, K. Hinds, and D. W. Grainer, Langmuir **12**, 5083 (1996).
[49] M. W. Tsao, C. L. Hoffmann, J. F. Rabolt, H. E. Johnson, D. G. Castner, C. Erdelen, and H. Ringsdorf, Langmuir **13**, 4317 (1997).
[50] A. J. Wagner, C. D. Vecitis, and D. H. Fairbrother, Surf. Sci. Spectra **8**, 32 (2001).
[51] C. Yan, A. Gölzhäuser, M. Grunze, and C. Wöll, Langmuir **15**, 2414 (1999).
[52] N. D. S. Canning, D. Outka, and R. J. Madix, Surf. Sci. **141**, 240 (1984).
[53] A. Krozer and M. Rodahl, J. Vac. Sci. Technol. A **15**, 1704 (1997).
[54] J. Huang and J. C. Hemminger, J. Am. Chem. Soc. **115**, 3342 (1993).
[55] P. E. Laibinis and G. M. Whitesides, J. Am. Chem. Soc. **114**, 9022 (1992).
[56] X. J. Dai, S. M. Hamberger, and R. A. Bean, Aust. J. Phys. **48**, 939 (1995).
[57] It should be noted that the RSO_3 species will also give rise to $O(1s)$ peaks between 531–532 eV, although calculations based on the relative concentration of the sulfonate species observed in the $S(2p)$ region indicate that changes in the $O(1s)$ region between 531–532 eV are dominated by the contribution from Au_2O_3.
[58] P. E. Laibinis, G. M. Whitesides, D. L. Allara, Y.-T. Tao, A. N. Parikh, and R. G. Nuzzo, J. Am. Chem. Soc. **113**, 7152 (1991).
[59] G. Liu, P. Fenter, C. E. D. Chidsey, F. D. Ogletree, P. E. Eisenberger, and M. Salmeron, J. Chem. Phys. **101**, 4301 (1994).
[60] R. J. Pace and S. I. Chan, J. Chem. Phys. **76**, 4241 (1982).
[61] J. Shen, V. Grill, and R. G. Cooks, J. Am. Chem. Soc. **120**, 4254 (1998).
[62] D. A. Hutt and G. J. Leggett, J. Phys. Chem. **100**, 6657 (1996).
[63] P. Andersen and A. C. Luntz, J. Chem. Phys. **72**, 5842 (1980).
[64] C. Gonzalez, J. J. M. MacDouall, and H. B. Schlegel, J. Phys. Chem. **94**, 7467 (1990).
[65] F. Ausfelder and K. G. McKendrick, Prog. React. Kinet. **25**, 299 (2000).
[66] T. T. Ehler, N. Malmberg, and L. J. Noe, J. Phys. Chem. B **101**, 1268 (1997).
[67] Z. Min, T.-H. Wong, H. Su, and R. Bersohn, J. Phys. Chem. A **104**, 9941 (2000).
[68] M. A. Golub and T. Wydeven, Polym. Degrad. Stab. **22**, 325 (1988).
[69] D. J. Wilson, A. J. Eccles, T. A. Steele, R. L. Williams, and R. C. Pond, Surf. Interface Sci. **30**, 36 (2000).
[70] K. Tanaka, T. Inomata, and M. Kogoma, Thin Solid Films **386**, 217 (2001).
[71] S. L. Koontz, L. J. Leger, J. T. Visentine, D. E. Hunton, J. B. Cross, and C. L. Hakes, J. Spacecr. Rockets **32**, 483 (1995).
[72] E. Murad, J. Spacecr. Rockets **33**, 131 (1996).
[73] S. Frey, K. Heister, M. Zharnikov, and M. Grunze, Phys. Chem. Chem. Phys. **2**, 1979 (2000).